The Role of Advection, Straining, and Mixing on the Tidal Variability of Estuarine Stratification

MALCOLM E. SCULLY

Center for Coastal Physical Oceanography, Old Dominion University, Norfolk, Virginia

W. ROCKWELL GEYER

Applied Ocean Physics and Engineering, Woods Hole Oceanographic Institution, Woods Hole, Massachusetts

(Manuscript received 23 November 2010, in final form 21 January 2012)

ABSTRACT

Data from the Hudson River estuary demonstrate that the tidal variations in vertical salinity stratification are not consistent with the patterns associated with along-channel tidal straining. These observations result from three additional processes not accounted for in the traditional tidal straining model: 1) along-channel and 2) lateral advection of horizontal gradients in the vertical salinity gradient and 3) tidal asymmetries in the strength of vertical mixing. As a result, cross-sectionally averaged values of the vertical salinity gradient are shown to increase during the flood tide and decrease during the ebb. Only over a limited portion of the cross section does the observed stratification increase during the ebb and decrease during the flood. These observations highlight the three-dimensional nature of estuarine flows and demonstrate that lateral circulation provides an alternate mechanism that allows for the exchange of materials between surface and bottom waters, even when direct turbulent mixing through the pycnocline is prohibited by strong stratification.

1. Introduction

Density stratification has a dominant influence on vertical mixing in estuaries and thereby has significant consequences for a wide array of estuarine processes. It plays a leading-order role in controlling the strength of the residual estuarine circulation (Hansen and Rattray 1965), impacts primary productivity by controlling the amount of time phytoplankton is retained in the photic zone (Lucas et al. 1998), modulates subpycnocline dissolved oxygen levels (Officer et al. 1984), and controls the transport of suspended particulate matter (Geyer 1993). Therefore, understanding the physical mechanisms that regulate vertical density stratification in estuaries is important to better understanding the biological and physical dynamics of these systems.

The influence of density stratification on turbulent mixing in estuaries has been clearly documented through field observations. Peters (1997) and Peters and Bokhorst (2000) documented intense turbulent mixing in the bottom boundary layer that was capped by the overlying density stratification. Only when the water column became well mixed did the boundary-generated turbulence extend throughout the water column. Trowbridge et al. (1999) found that the local departure from the law of the wall relationship was greater than expected based on the local stratification and concluded that the suppression of the turbulent length scale from the overlying stratification limited turbulent mixing in the underlying boundary layer. These studies clearly demonstrate that both the vertical location and intensity of vertical density stratification play an important role in governing turbulent mixing in estuaries.

At tidal time scales, variations in vertical salinity stratification are usually assumed to be dominated by the interaction between the along-channel salinity gradient and the vertical shear in the along-channel velocity, a process known as tidal straining (Simpson et al. 1990). This process tends to favor the development of stratification during ebb tides and the destruction of stratification during the flood. The variations in stratification attributed to this mechanism have been shown to lead to significant tidal asymmetries in turbulent mixing (Jay and

Corresponding author address: Malcolm E. Scully, Center for Coastal Physical Oceanography, Old Dominion University, 4111 Monarch Way, Norfolk, VA 23508.
E-mail: mscully@odu.edu

DOI: 10.1175/JPO-D-10-05010.1

Smith 1990; Nepf and Geyer 1996; Stacey et al. 1999; Geyer et al. 2000; Rippeth et al. 2002; Simpson et al. 2005; Stacey and Ralston 2005; Chant et al. 2007). Significant attention has focused on the role that tidal asymmetries in turbulent mixing have on the creation of the tidally averaged estuarine circulation (Jay and Musiak 1994; Stacey et al. 2001; Scully and Friedrichs 2007; Burchard and Hetland 2010). These studies suggest that the circulation driven by tidal nonlinearities in mixing is equally, if not more, important than the more traditionally assumed baroclinically driven flow.

Implicit in most of these studies is the assumption that stratification is larger during the ebb phase of the tide than during the flood. This assumption assumes that vertical gradients in the horizontal salinity gradient are weak (or equivalently that the horizontal gradients of stratification are weak) and ignores the role of lateral circulation. However, all stratified estuaries must have some vertical variation in the longitudinal salinity gradient to satisfy the requirement of well-mixed conditions upstream from the head of salt. This is most apparent in strongly stratified salt wedge estuaries, where the length of the salinity intrusion is often comparable to the tidal excursion. In such systems, along-channel advection of the salinity structure contributes to tidal variations in stratification at first order (Giddings et al. 2011).

The role of lateral processes in controlling stratification in estuaries also has been largely ignored. This is surprising given that the full three-dimensional nature of flows has long been recognized to play an important role in along-channel dispersion (Taylor 1954; Aris 1956; Elder 1959; Fisher 1976). Only recently has the role that lateral circulation plays in controlling stratification in an estuary been directly addressed. Lacy et al. (2003) demonstrated that strong lateral density gradients interact with the lateral circulation they generate to play an important role in governing vertical density stratification in northern San Francisco Bay. Their results demonstrate that lateral circulation can provide a mechanism for generating stratification during the flood tide and that this process has significant impact on the timing and intensity of turbulent mixing. Scully and Friedrichs (2007) demonstrated that the classic pattern of longitudinal tidal straining held at a location in the deepest portion of the estuarine cross section but that shallower adjacent regions demonstrated the opposite pattern, with greater stratification during flood than during ebb tide. They inferred that the timing and intensity of turbulent mixing exhibited significant variability because of the tidal and lateral variability in stratification. These results suggest that along-estuary tidal straining does not adequately represent the tidal variations in stratification and that lateral processes can play an important role in the control of stratification and mixing.

In this paper, we use observations collected from the Hudson River estuary to demonstrate that the tidal variability in stratification is more complicated than the traditionally assumed model of along-channel tidal straining. Advection of both along- and across-estuary gradients in stratification, transverse tidal straining, and asymmetries in tidal mixing all contribute significantly to the tidal evolution of estuarine stratification. As a result, large regions of the estuarine cross section exhibit tidal variations in stratification that are opposite of that predicted by longitudinal tidal straining. These data demonstrate the three-dimensional nature of estuarine stratification and highlight the importance of lateral transport processes to vertical exchange in estuaries. The field experiment and analytical methods are described in section 2. The results are presented in section 3, including a detailed description of the spatial and temporal patterns of stratification and circulation, evaluation of the relative roles of horizontal straining and advection of stratification, and the role of turbulent mixing. This is followed in section 4 by a discussion of the implications that the observed patterns in stratification and turbulent mixing have on vertical exchange in stratified estuarine systems.

2. Methods

a. Hudson River field experiment, October 2006

A 5-day experiment was conducted on the Hudson River during October 2006, during spring tides and elevated river discharge conditions (~900 $m^3 s^{-1}$). The experiment focused on a region 20 km up estuary from the Battery in Manhattan, New York (Fig. 1). A combination of both moored instrumentation and shipboard observations were collected during the experiment. The moored instrumentation consisted of a bottom-mounted acoustic Doppler current profiler (ADCP) and profiling conductivity–temperature–depth (CTD) winch, which were both deployed in approximately 8 m of water halfway between the deepest portion of the channel and the western shore (Fig. 1). The ADCP was an RD Instruments 1200-kHz broadband workhorse that sampled every 2 s, recording data in 25-cm bins. The ADCP provided vertical profiles of velocity for the first 3 days of the experiment. The CTD profiling system consisted of a bottom-mounted winch connected to a Seabird Electronics SBE-19 CTD. The winch released the CTD every 30 min, allowing it to ascend buoyantly to the surface. Once at the surface, the bottom-mounted winch retrieved the cable completing the vertical cast.

To complement the moored instrumentation, 4 consecutive days of shipboard observations were collected

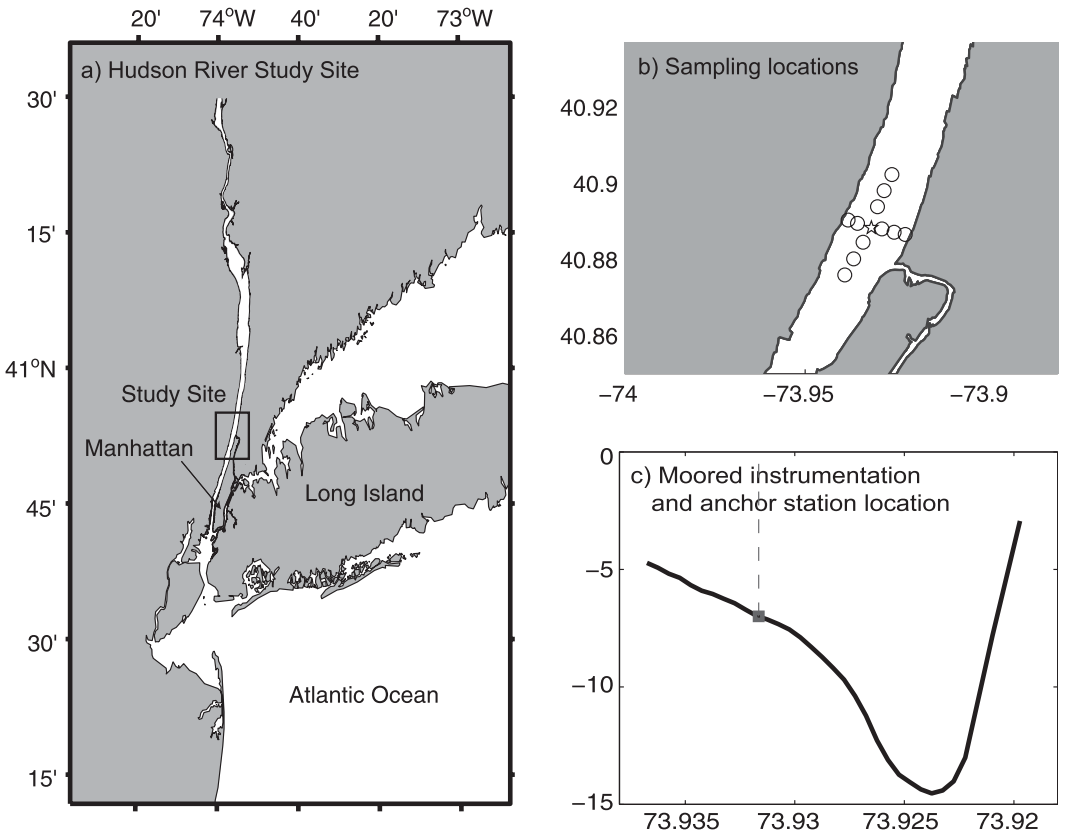

FIG. 1. (a) Site map of Hudson River study site. (b) Locations of longitudinal and lateral sampling locations. The star denotes the location of the moored ADCP and profiling CTD. (c) Position of the moored ADCP and profiling CTD in estuarine cross section.

from the R/V *Tioga* and R/V *Mytilus*. The R/V *Tioga* deployed the Mobile Array for Sensing Turbulence (MAST). The MAST is a 10-m rigid pole that is deployed vertically from a crossbar that mounts across the bow of a research vessel (for details, see Geyer et al. 2008). For this experiment, the MAST contained sox vertically adjacent instrument brackets with three collocated sensors: 1) a Sontek acoustic Doppler velocimeter (25 Hz); 2) a Seabird Electronics SBE-7 microconductivity probe (300 Hz); and 3) an RBR CTD sensor (6 Hz). The fast-response microconductivity probes (SBE-7s) did not function properly during this experiment and will not be discussed. In addition to the MAST, the R/V *Tioga* also had a downward-looking 1200-kHz ADCP that sampled every 2 s with a bin spacing of 25 cm.

The R/V *Tioga* employed two different modes of operation over the four days. On 21 and 23 October, the *Tioga* occupied a fixed anchor station located on the western shoal immediately adjacent to the moored instrumentation (Fig. 1). During the fixed anchor station deployments, a three-point mooring maintained the vessel position, facing into the along-channel flow. On each day, the fixed anchor station was occupied for 13 h and the vessel was repositioned after 6 h, when tidal currents reversed. On 22 and 24 October, the MAST was used to occupy six laterally adjacent stations spanning the estuarine cross section. At each station, the *Tioga* held position for 5 min, facing into the along-channel current. During peak tidal currents, the vessel could hold a relatively fixed position over ground. However, during weak tidal currents, the vessel had to move forward over ground in order to maintain steerage. The lateral stations were occupied sequentially, with repeated surveys conducted approximately every hour for a complete tidal cycle (~13 h).

The R/V *Mytilus* provided high-resolution axial and lateral CTD surveys. On 21, 23, and 24 October, the *Mytilus* occupied the stations indicated on Fig. 1, collecting CTD profiles. The axial stations were occupied sequentially, followed by the lateral transect with a repeat interval of approximately 1 h, providing relatively high-resolution characterization of the estuarine density field. To characterize the larger-scale estuarine salinity field, the R/V *Mytilus* conducted a slack water longitudinal survey along the deepest portion of the channel

from just south of the Battery to the head of salt (Croton Point in Haverstraw Bay) on 22 October 2006, providing a roughly synoptic view of the larger-scale along-channel salinity distribution.

b. Data analysis

The analysis in this paper employs a right-hand coordinate system with the x axis directed along the main channel of the estuary where positive along-channel flow u is defined as flood directed. The y axis is horizontally orthogonal to the along-channel axis, with positive transverse flow v directed toward the west. Vertical flow w along the z axis is positive upward, and $z = 0$ corresponds to the tidally averaged position of the sea surface. Using this coordinate system and neglecting the horizontal divergence in turbulent salt flux, the equation for conservation of salt S can be written as

$$\frac{\partial S}{\partial t} = -u\frac{\partial S}{\partial x} - v\frac{\partial S}{\partial y} - w\frac{\partial S}{\partial z} + \frac{\partial}{\partial z}\langle S'w'\rangle. \tag{1}$$

The terms on the right-hand side are along-channel advection, lateral advection, vertical advection, and the divergence in the vertical turbulent salt flux, respectively. The angled brackets and primes are used to indicate Reynolds-averaged and turbulent fluctuations, respectively. Taking the vertical derivative of (1) provides an equation that describes the evolution of the vertical salinity gradient,

$$\underset{\text{(A)}}{\frac{\partial}{\partial t}\frac{\partial S}{\partial z}} = \underset{\text{(B)}}{-\frac{\partial u}{\partial z}\frac{\partial S}{\partial x}} \underset{\text{(C)}}{- u\frac{\partial}{\partial x}\frac{\partial S}{\partial z}} \underset{\text{(D)}}{- \frac{\partial v}{\partial z}\frac{\partial S}{\partial y}} \underset{\text{(E)}}{- v\frac{\partial}{\partial y}\frac{\partial S}{\partial z}} \underset{\text{(F)}}{- \frac{\partial w}{\partial z}\frac{\partial S}{\partial z}} \underset{\text{(G)}}{- w\frac{\partial^2 S}{\partial z^2}} + \underset{\text{(H)}}{\frac{\partial^2}{\partial z^2}\langle S'w'\rangle}. \tag{2}$$

Vertical differentiation of the horizontal advective terms in Eq. (1) result in two terms: 1) the straining term, which represents the interaction between vertical shear and horizontal salinity gradients (terms B and D), and 2) the horizontal advection of the vertical salinity gradient (terms C and E). Horizontal advection of stratification occurs when there are horizontal gradients in $\partial S/\partial z$. Vertical velocities also alter the local value of $\partial S/\partial z$, either by compressing or expanding the vertical salinity gradient (term F) or through vertical advection of vertical gradients in $\partial S/\partial z$ (term G). Finally, stratification can be reduced through turbulent mixing (H).

The traditional model for along-channel tidal straining only accounts for one of the six advective terms in Eq. (2): term B. A primary goal of this paper is to evaluate the relative importance of both longitudinal and lateral straining, as well as the importance of horizontal advection of stratification. This will be done using the moored ADCP data in conjunction with vessel surveys. To provide simultaneous estimates of both the longitudinal and lateral salinity gradients, data collected at each adjacent station were interpolated in time to match the sample time of the central station (the ADCP location). The data from each CTD cast were interpolated to match the fixed vertical coordinates of the moored ADCP data, accounting for the changes in tidal elevation. These data will be used to quantify the first four terms on the right-hand side of Eq. (2). Because of the time variations in sea surface height and the loss of near-surface ADCP data due to side-lobe contamination, the terms in Eq. (2) could not be estimated very near the surface. Further, the depth of the shallowest laterally adjacent CTD station (~6 m) limits the depth to which the lateral salinity gradient can be estimated. As a result, no estimates of the lateral advective terms are available for the region 1.5–2 m above the bed (mab). Velocity data near the bed also are limited because the lowest bin of ADCP is roughly 1 mab. The vertical velocity measurements from the ADCP were not of sufficient quality to resolve the vertical advective terms in (2), and direct estimates of turbulent salt flux were not available. It is important to note that most of the terms in Eq. (2) involve measurements of velocity and salinity collected from different instrument platforms. The instruments were not precisely collocated, and most terms involve spatial derivatives obtained from finite differencing. As a result, there are significant uncertainties inherent in these observations, and the results should be viewed as order of magnitude estimates of the terms.

The data from the MAST are used to examine the influence of stratification on turbulent mixing. The MAST provides highly resolved estimates of the gradient Richardson number (Ri),

$$\mathrm{Ri} = \frac{N^2}{[(\partial u/\partial z)^2 + (\partial v/\partial z)^2]}, \tag{3}$$

where $N^2 = -(g/\rho_0)(\partial\rho/\partial z)$. Estimates of Ri were based on 5-min averages of the observed velocity and density fields. For an estuarine flow, 5 min is long compared to the generation time scale of turbulence but short enough to be considered steady relative to the tidal acceleration. Data from the MAST also were used to calculate the

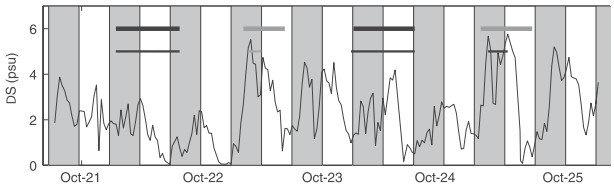

FIG. 2. Top-to-bottom salinity difference observed by the profiling CTD winch. Shaded regions indicate flood tides. Horizontal lines indicate ship-based sampling periods. The thick black line indicates R/V *Tioga* anchor stations and the thick gray line indicates R/V *Tioga* lateral surveys. The thin black line indicates local longitudinal and lateral surveys by R/V *Mytilus*. The thin gray line indicates the Battery to head of salt longitudinal survey by R/V *Mytilus*.

dissipation rate ε of turbulent kinetic energy (TKE) following the methodology outlined in Scully et al. (2011). This method involves fitting a theoretical spectrum to the vertical velocity spectrum and is analogous to the inertial dissipation method (Grant et al. 1984), with the advantage that contamination due to instrument noise is effectively removed (for details, see Scully et al. 2011). Turbulence measurements from the MAST are used to estimate the relative importance of turbulent mixing to the observed evolution of stratification.

3. Results

a. Salinity stratification

The bottom-mounted profiling CTD provided a time series of top-to-bottom salinity stratification over the duration of the experiment (Fig. 2). Large changes in stratification are observed at tidal time scales, ranging from nearly well mixed to top-to-bottom differences of nearly 6 psu. In general, the stratification decreases throughout the ebb and increases during the flood, with values of maximum stratification usually observed at the end of the flood tide. To examine the progression of vertical salinity profiles through the tidal cycle, all of the profile data were averaged as a function of tidal phase (Fig. 3). During the flood, the bottom layer gets progressively saltier and the near-bed well-mixed region grows slightly in the vertical. However, the surface salinities do not increase as rapidly and the overall stratification increases throughout the flood. At the beginning of the ebb tide, strong stratification from the previous flood tide is observed. However, this stratification decreases rapidly, particularly during the second half of the ebb tide.

The profiling CTD provides a highly resolved time series, but only at one location in the estuarine cross section. Data from the lateral CTD surveys provide the lateral structure of the salinity field as it evolves over the tidal cycle (Fig. 4). During the early stages of the flood tide, the salinity stratification is largely located over the deeper channel areas, with lower values of top-to-bottom salinity difference observed over the western shoal. As the flood tide progresses, stratification near the bed in the deep channel areas is reduced, but the pycnocline is intensified over the western shoal and higher in the water column over the deep channel. During the early stages of the flood tide, the lateral distribution of salinity is consistent with the pattern expected because of lateral differential advection (Nunes and Simpson 1985). However, as the flood tide progresses, the halocline tilts downward to the east, consistent with the expected response via thermal wind, reversing the lateral salinity gradient. At the beginning of the flood tide, there is a lateral gradient in stratification, with regions of strong

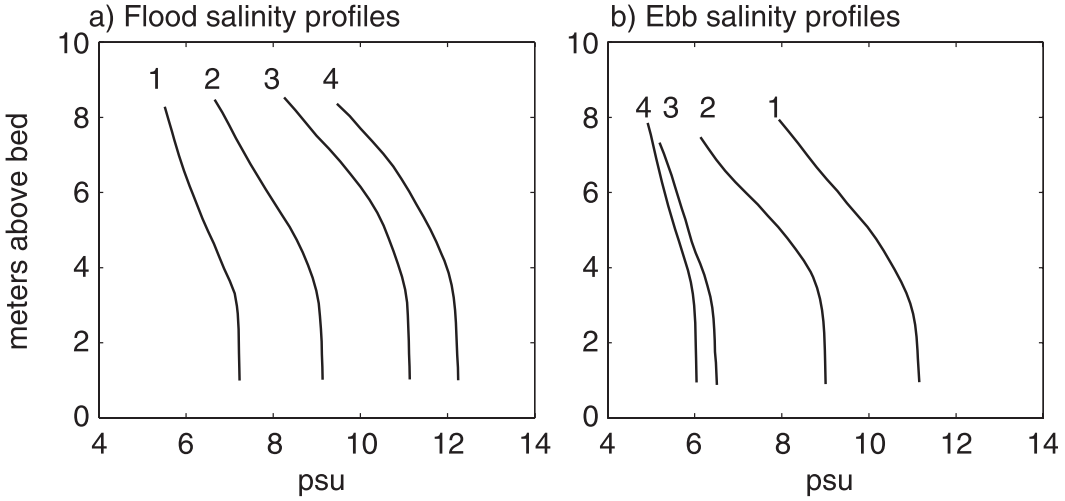

FIG. 3. Vertical profiles of salinity from profiling CTD winch for (a) flood and (b) ebb tides. Values have been averaged as a function of tidal stage for the entire deployment. Numbers indicate the progression through the tidal cycle.

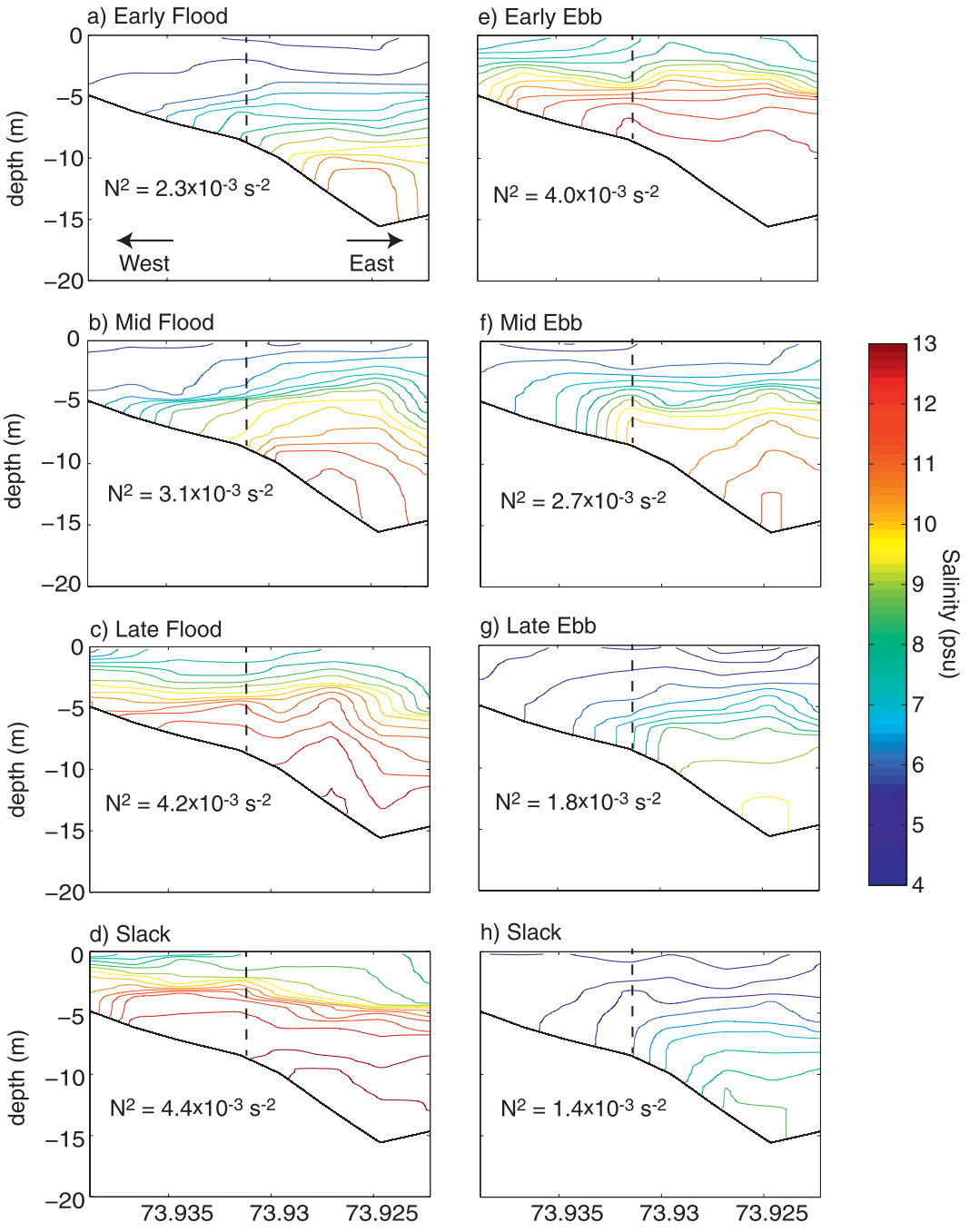

FIG. 4. Tidal evolution of transverse salinity structure from CTD surveys conducted on 23 Oct 2006. The contour interval is 0.5 psu. For each plot, the cross-sectionally averaged value of N^2 is reported. The dashed vertical line indicates the location of the profiling CTD and bottom-mounted ADCP.

stratification located over the deeper channel. As the flood tide progresses, the stratification over the western shoal intensifies. This increase in stratification over the western shoal is consistent with lateral advective processes, which may provide a mechanism for the increased stratification observed by the profiling winch during flood tides throughout the experiment. At the beginning of the ebb tide, the strong stratification over the shoal remains and there is a relatively well-mixed near-bed region near the bed in the channel. During the ebb tide, the strong stratification over the western shoal is rapidly reduced, whereas the stratification increases slightly over the near-bed region in the deep channel.

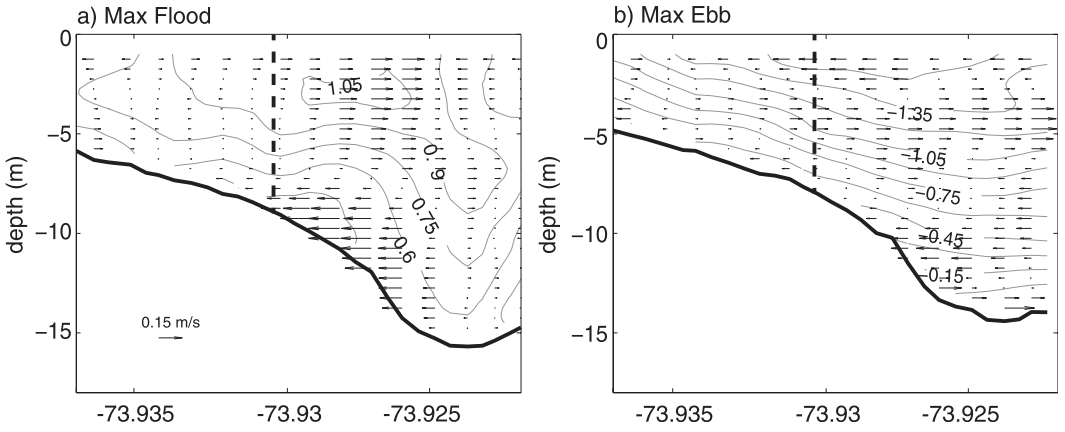

FIG. 5. Cross-sectional distribution of horizontal velocity at (a) maximum flood and (b) maximum ebb collected with a downward-looking ADCP during across-channel surveys on 24 Oct 2006. Along-channel velocity is contoured with a 0.15 m s^{-1} contour interval. Lateral velocities are depicted with arrows. The dashed vertical line indicates the position of the moored ADCP.

These data are not consistent with the traditional model of tidal straining: the cross-sectionally averaged value of N^2 generally increases during the flood and decreases during the ebb (Fig. 4). Only in the bottom boundary layer of the deep channel is the stratification observed to increase during the ebb and decrease during the flood. The shoal region exhibits the greatest changes in stratification over the tidal cycle, increasing by over a factor of 5 during the flood tide. This large increase in stratification that is generated during the flood is largely erased during the following ebb tide.

b. Tidal circulation

The CTD surveys suggest that one potential mechanism driving the restratification over the western shoal during the flood tide is lateral circulation. The lateral surveys with the ship-mounted ADCP provide a detailed view of the spatial distribution of both the along- and across-channel circulation (Fig. 5). Data for maximum flood and maximum ebb are plotted separately using the data collected on 24 October. During the flood tide, there is pronounced lateral shear in the along-channel flow, and the across-channel flow is vertically sheared with strong near-bed velocities direct toward the western shore (~0.15 m s^{-1}). The two-layer lateral flow is intensified in the transition region in between the deeper channel and adjacent shoal. In contrast, the lateral flow during the ebb is significantly reduced and exhibits a more complex three-layer structure. This asymmetry in the strength of the lateral flow has been noted in both idealized estuarine modeling simulations (Lerczak and Geyer 2004), as well as in previous modeling studies of the Hudson River (Scully et al. 2009). These previous studies demonstrate that the lateral momentum balance is largely geostrophic at tidal time scales, and the enhanced lateral circulation observed during the flood tide occurs when differential advection of the along-channel salinity gradient breaks the thermal wind balance. Although the data collected in this experiment are not sufficient to adequately characterize the lateral momentum balance, the general patterns are consistent with these previous studies.

The bottom-mounted ADCP demonstrates that the tidal asymmetry in the lateral flow is a persistent feature over the shoal location (Fig. 6). Over the entire deployment, strong lateral flows develop during the second

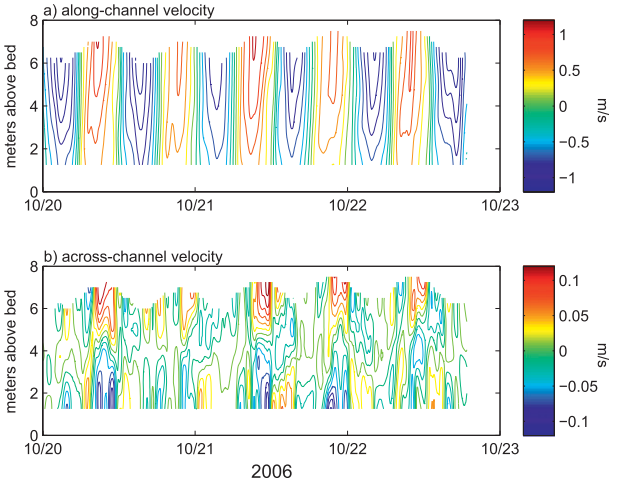

FIG. 6. Contours of (a) along-channel and (b) across-channel velocity collected by the bottom-mounted ADCP. The contour interval for along-channel velocity is 0.20 m s^{-1} and positive values indicate flood currents. The contour interval for across-channel velocity is 0.02 m s^{-1} and positive values indicate a lateral flow toward the eastern shore.

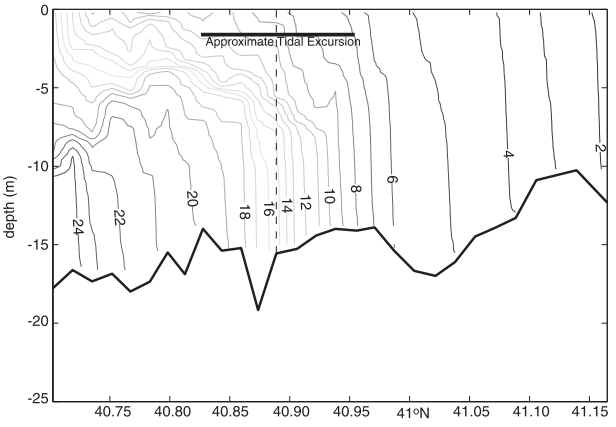

FIG. 7. Along-channel salinity contours from survey on 22 Oct 2006. The survey was conducted during slack currents following a flood tide. The salinity contour interval is 1 psu, and the dashed vertical line represents the approximate along-channel location of moored instrumentation, anchor stations, and lateral surveys. The thick horizontal line represents the approximate tidal excursion (~13 km). The survey began at Battery Park (~40.70°N) and ended at Croton Point (~41.17°N).

half of the flood tide, with flow near the bed directed to the west and flow near the surface directed to the east, consistent with bottom Ekman dynamics. The sense of the vertical shear in the lateral flow reverses during the early ebb but is reduced somewhat in magnitude. As seen in Fig. 4, there is a strong lateral gradient in stratification at slack before flood. As the flood tide progresses, the strong lateral flow provides a mechanism for advecting stratified water from the channel onto the western shoal. The location of where the pycnocline intersects the bottom can be thought of as a bottom salinity front, separating the more stratified water in the channel from the less stratified water on the shoal. As the flood tide progresses, this near-bed front advances westward across the shoal region and, as a result, the lateral advection of stratification (term E) acts to increase stratification at this location.

c. Along-channel salinity structure

The observations presented above demonstrate strong lateral circulation and strong lateral gradients in both salinity and stratification, suggesting that lateral processes may play an important role in the evolution of stratification. The slack water along-channel survey conducted on 22 October also demonstrates significant along-channel variability in stratification (Fig. 7). The region up estuary from the instrumented cross section generally has less top-to-bottom salinity stratification as compared to the more stratified down-estuary region. As a consequence of this spatial variability, the along-channel advection of stratification acts to reduce stratification during the ebb and increase stratification during the flood. Thus, the advection of stratification appears to be acting in opposition to the tidal patterns favored by along-channel straining. Although the along-channel salinity field in Fig. 7 is approximately synoptic with respect to tidal phase, this structure may be significantly modified during the tidal cycle. To quantify the relative importance of both the straining and advection terms in the longitudinal and lateral direction, we use the intensive tidal cycle CTD surveys in conjunction with the moored ADCP data.

d. Estimates of the advective and straining terms

The CTD surveys and moored ADCP provide the data necessary to quantify both the horizontal straining terms and the horizontal advection of stratification at the central instrument location. Consistent with the measurements collected by the profiling CTD, the survey data show that depth-averaged value of $\partial S/\partial z$ generally increases during the flood and decreases during the ebb (Fig. 8a). To examine the processes responsible for these variations, vertical profiles of the horizontal straining and advection terms in Eq. (2) are plotted (Figs. 8b,c), averaged separately over the flood and ebb tides. As expected, along-channel straining (term B) acts to increase and decrease $\partial S/\partial z$ throughout the water column on ebb and flood tide, respectively. During the flood tide, the longitudinal advection of $\partial S/\partial z$ (term C) acts to increase $\partial S/\partial z$ over the lower half of the water column and decrease $\partial S/\partial z$ near the surface. The longitudinal advection term is larger and has the opposite sign from the straining term over the lower half of the water column. Higher in the water column, longitudinal advection augments longitudinal straining. During the ebb tide, along-channel advection brings less stratified water from up estuary, acting to decrease $\partial S/\partial z$ through most of the water column.

During the flood tide, the lateral straining term (term D) is positive near the surface and near the bottom but switches sign in the middle of the water column. In a depth-averaged sense, the longitudinal straining and lateral straining terms are of the same order of magnitude. Early in the flood, the water in the channel is saltier than over the shoal. However, as the flood tide progresses, the halocline tilts downward toward the west, consistent with the thermal wind response to the vertical shear in the along-channel flow. This reverses the salinity gradient in the middle water column and combined with the strong vertical shear in the lateral flow acts to reduce $\partial S/\partial z$ in the middle portion of the water column during the flood tide. Both the vertical shear in the lateral flow and lateral salinity gradient switch sign during the ebb so that the lateral straining term has

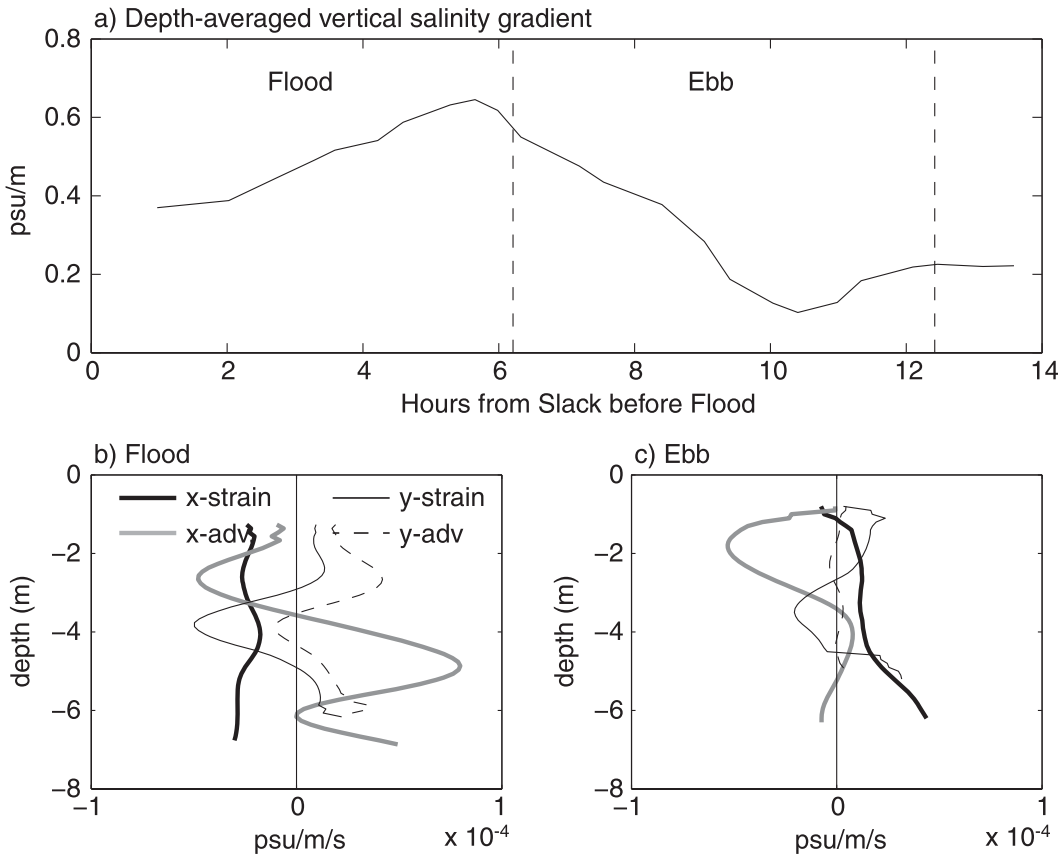

FIG. 8. (a) Time series of depth-averaged vertical salinity gradient observed at the central CTD station during the 21 Oct surveys. Comparison of profiles of the horizontal advection and straining terms from Eq. (2) averaged over (b) flood and (c) ebb tides, plotted as a function of depth. The thick black line represents longitudinal straining (term B), the thick gray line represents longitudinal advection (term C), the thin black line represents transverse straining (term D), and the dashed line represents transverse advection (term E).

a similar vertical distribution on flood and ebb. During ebb, the lateral advection of $\partial S/\partial z$ (term E) is generally an order of magnitude lower than the other terms. That is not the case during the flood tide, when term E is of similar magnitude to both along-channel advection and along-channel straining. As discussed in section 3b, the positive values of term E are consistent with the lateral advance of a bottom salinity front across the western shoal during the flood tide.

During the flood tide, the net horizontal terms do not closely match the observed changes in stratification (Fig. 9a). Over the lower portion of the water column, the observed time rate of change of $\partial S/\partial z$ is generally less than predicted by the sum of the horizontal terms. In contrast, the observed time rate of change of $\partial S/\partial z$ is greater than the horizontal terms in the upper portion of the water column. Although our data are not sufficient to quantify the vertical velocity, the mismatch between the observed changes in stratification and the sum of the horizontal terms is generally consistent with vertical processes. The strong lateral flows that advect stratified water westward across the shoal during the flood tide most likely vertically lift the salinity field (term G). In fact, in the fixed coordinate system used in this analysis, the sloping bottom requires a positive vertical velocity near the bed on flood tide if there is no along-channel divergence in the flow. The observed vertical gradient in $\partial S/\partial z$ combined with a positive vertical velocity would generally decrease $\partial S/\partial z$ near the bed and increase $\partial S/\partial z$ near the surface during flood tide, a pattern that is generally consistent with the observed mismatch depicted in Fig. 9a.

During ebb, there is reasonable agreement between the observed rate of change in stratification and the net horizontal terms in the upper half of the water column (Fig. 9b). This agreement suggests that vertical advection plays a smaller role during the ebb tide. Simple arguments that invoke the continuity relation would suggest weaker vertical velocities during the ebb, when the lateral circulation is suppressed. During ebb, the

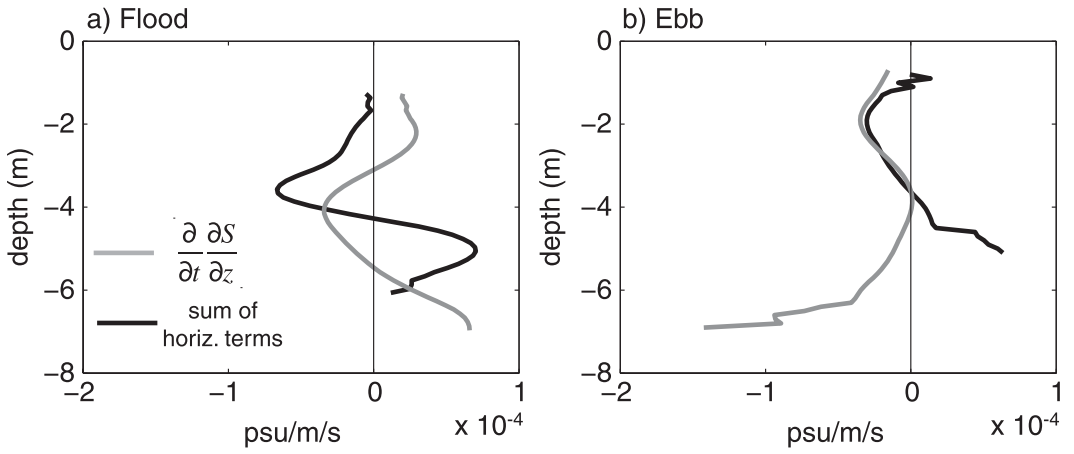

FIG. 9. Vertical profiles of the observed time rate of change of vertical salinity gradient (gray line) and the sum of the horizontal terms (B + C + D + E) in Eq. (2) (black line), averaged over (a) flood and (b) ebb tide, plotted as a function of depth. The mismatch near the bed during ebb tide is consistent with the destruction of stratification by vertical mixing. Profiles of the horizontal terms are limited by the depth of the laterally adjacent shoal station, preventing comparison with the observed time rate of change in the region closest to the bed.

greatest divergence between the observed rate of change in stratification and the net horizontal terms is near the bed. Over the lower portion of the water column, the sum of the horizontal terms from Eq. (2) favors the increase in $\partial S/\partial z$, whereas the observations demonstrate a reduction in stratification. Although this could be the result of vertical advection, this mismatch is consistent with the destruction of $\partial S/\partial z$ via vertical mixing.

e. *Tidal variations in turbulent mixing*

The anchor station data collected with the MAST provide evidence that turbulent mixing is limited during the flood tide, whereas strong turbulent mixing during the ebb tide contributes to the observed reduction in stratification. During the flood tide, the stratification that develops maintains the gradient Richardson number above its critical value over much of the water column (Fig. 10a). During the period of peak flood currents, there is a relatively thin (<3 m) near-bed region where values of Ri are below 0.25. Elevated values of dissipation are largely limited to this bottom boundary layer where Ri < 0.25 (Fig. 10b). As the ebb tide begins, the stratification caps the growth of the bottom boundary layer, limiting intense turbulent mixing to the near-bed region. However, as the ebb progresses, the stratification is significantly reduced and values of Ri are below 0.25 throughout the water column. During this period, elevated dissipation extends nearly to the surface, suggesting a boundary layer that occupies the full water depth.

The reduction in stratification and higher dissipation rates observed during the ebb tide are indicative of intense vertical salt flux over the western shoal region. The data collected with the MAST can be used to estimate the relative importance of turbulent mixing to the observed stratification. In the Hudson River, the vertical gradients in salinity are significantly larger than those due to temperature. As a result, the buoyancy flux B can be approximated as $B \sim g\beta\langle s'w'\rangle$, where g is the gravitational constant and β is the haline expansion coefficient ($\sim 7.8 \times 10^{-4}$ psu^{-1}). Relating the observed values ε to B via the flux Richardson number (Rf $\sim B/\varepsilon$) gives a simple scaling relationship for the reduction in stratification across a layer of thickness H_L, via turbulent mixing,

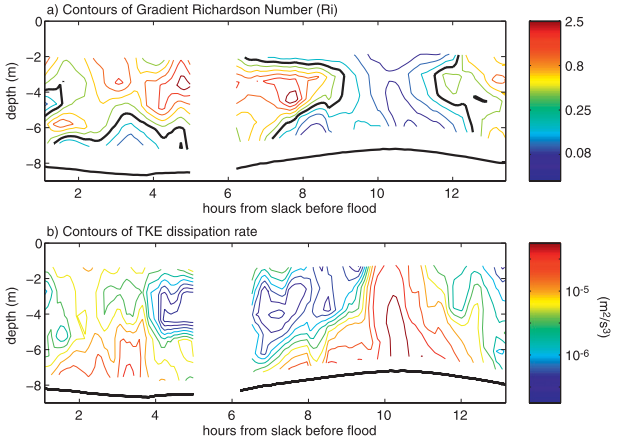

FIG. 10. (a) Contours of the gradient Richardson number Ri estimated from the MAST data collected on 23 Oct 2006 (log scale). Heavy black contour corresponds to Ri = 0.25. (b) Contours of the dissipation rate of TKE estimated from the vertical velocity spectrum from MAST acoustic Doppler velocimeter (ADV) data (log scale). The ship had to be repositioned to ensure that the sensors faced into the current causing the gap in data around hour 5.

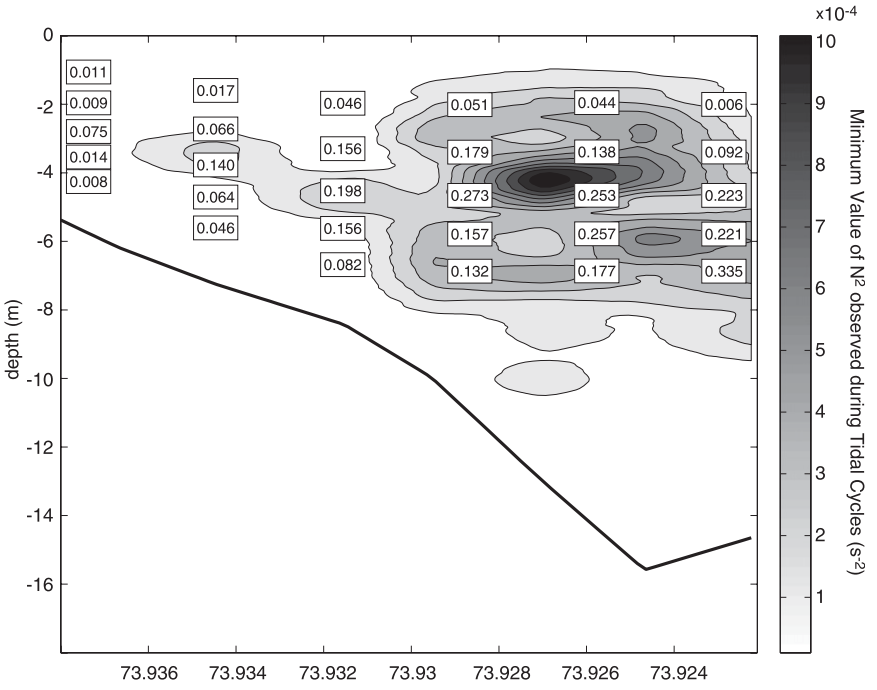

FIG. 11. Minimum values of the gradient Richardson number Ri observed over two tidal cycles superimposed on contours of the minimum value of N^2 observed over two tidal cycles. Values of Ri are derived from lateral surveys with the MAST, and values of N^2 are derived from lateral CTD surveys. At the three eastern locations, where persistent stratification was maintained, values of Ri did not drop below 0.25 over the course of two tidal cycles.

$$\frac{\partial^2}{\partial z^2}\langle s'w'\rangle \approx \frac{B}{g\beta H_L^2} \approx \frac{\varepsilon Rf}{g\beta H_L^2}. \tag{4}$$

At peak flood and ebb currents, average values of ε estimated from the MAST in the middle of the water column are approximately 1×10^{-5} and 5×10^{-5} m^2 s^{-3}, respectively. Assuming that $H_L \sim 3$ m and Rf ~ 0.15 (Osborn 1980; Oakley 1982; Moum 1996) gives values for the reduction in stratification due to turbulent mixing of approximately 0.3×10^{-4} and 1.5×10^{-4} psu m^{-1} s^{-1} for flood and ebb, respectively. During the ebb tide, this would result in approximately a 3-psu reduction in top-to-bottom salinity difference over the duration of the tidal cycle, largely consistent with observations. In contrast, the factor of 5 smaller mixing rate during the flood tide is not sufficient to overcome the straining and advection terms, resulting in the observed increase in stratification.

The near-complete reduction of stratification during the ebb tide at the shoal location is not observed over the deeper channel areas, where persistent stratification is maintained throughout the tidal cycle. The lateral transects collected with the MAST were used to calculate the minimum value of Ri that was observed at multiple stations in the estuarine cross section over two complete tidal cycles (Fig. 11). The values of Ri are superimposed on the minimum value of N^2 that was calculated from the two complete tidal cycles of lateral CTD profiles. At the three westernmost sites, the minimum value of Ri at all locations in the water column fell below 0.25, generally during the ebb tide. In contrast, at the three easternmost sites over the deep channel area, persistent stratification is maintained and there was at least one location within the water column where the value of Ri never was observed to fall below 0.25 over the two complete tidal cycles.

At the shoal location where the bottom-mounted ADCP was deployed, the tidally averaged near-bed estuarine velocity was directed down estuary (data not shown). As a result, we infer that the greater mixing during the ebb tide is the result of higher bed stress during ebb at this location. In contrast, the tidally averaged estuarine velocity is flood directed in the deeper parts of the main channel. At these locations the bed stress is greater during the flood tide, with enhanced flood mixing as documented by the dye studies of Chant et al. (2007) and the microstructure observations of Peters and Bokhorst (2000).

4. Discussion and implications

The observations presented above document that the tidal variation in stratification along the western shoal of

the upper Hudson River are not consistent with the expected variability due to along-channel tidal straining. Along-channel advection (term C), lateral advection (term E), and tidal asymmetries in turbulent mixing (term H) all contribute to the observed deviations from the expected patterns in stratification at this location. It is likely that the relative importance of all three of these processes is amplified at the particular site where these observations were collected. At this location, both the along- and across-channel advection of horizontal gradients $\partial S/\partial z$ contribute to the evolution of stratification. The original derivations of subtidal estuarine dynamics assume that $\partial S/\partial x$ is constant in the vertical (e.g., Hansen and Rattray 1965). However, Chatwin (1976) points out that this assumption is only valid when

$$\frac{\partial S}{\partial x} \gg \frac{48 U_r A_z}{g\beta H^3}, \tag{5}$$

where U_r is the velocity associated with the river discharge and A_z is the vertical eddy viscosity. This is analogous to saying that vertical gradients in $\partial S/\partial x$ can only be ignored when the ratio of the river velocity to the estuarine residual velocity U_E is much smaller than unity. Assuming the Hansen and Rattray (1965) scaling for U_E in conjunction with Knudsen's theorem (Proudman 1953), Eq. (5) can be rearranged to provide simple constraint on when it is appropriate to ignore vertical variations in $\partial S/\partial x$,

$$\frac{U_r}{U_E} \sim \frac{\Delta S}{\langle S \rangle} \ll 1, \tag{6}$$

where ΔS is the top-to-bottom salinity difference and $<S>$ is the vertically averaged salinity. Clearly, as river discharge and stratification increase, this assumption is not valid. Further, this condition cannot be satisfied near the head of salt, where the residual estuarine velocity approaches zero by definition.

The observations presented in this paper were collected during spring tidal conditions and during a period of elevated river discharge. The stronger tidal mixing associated with spring tides tends to reduce U_E, and higher river discharge increases U_r. Further, the observations were collected well above the central region of the estuary, where the assumption that $\partial S/\partial x$ is constant in the vertical is most valid. All of these factors amplify horizontal gradients in $\partial S/\partial x$. However, it is important to note that the assumption that $\partial S/\partial x$ is constant in the vertical is not valid for much of the Hudson River under moderate flow conditions (Fig. 7) and most estuaries with strong river forcing. As a result, the importance of longitudinal advection on stratification is likely to be important in all estuaries with significant river flow.

It is likely that the role of lateral advection (term E) also is amplified at the western shoal location that is the focal point of this study. Both lateral gradients in $\partial S/\partial z$ and tidal asymmetries in the strength of the transverse circulation are pronounced at this location. This is largely the result of lateral variations in estuarine bathymetry, which favors higher bed stress in the deeper channel areas during flood tides and higher bed stress over the shoals during ebb. The strong mixing during the ebb tide allows boundary-generated turbulence to extend throughout the water column and the vertical stratification is largely erased. In contrast, over the deeper channel regions, persistent stratification is maintained and the boundary layer does not grow to occupy the full water column. This results in a strong lateral gradient in $\partial S/\partial z$ at the end of ebb tide at this location, which is near the general location of a frontal feature that separates the relatively well-mixed water over the shoal from the more stratified water over the channel. The more stratified water adjacent to this location is then laterally advected onto the shoal by the strong lateral circulation that develops during flood tide. The overall importance of this mechanism is enhanced by the strong tidal asymmetry in lateral flow at this location. As seen in Fig. 5, the strong tidal asymmetry in lateral flow is less pronounced at other locations in the estuarine cross section.

Although the role of lateral advection may be reduced at other locations in the cross section, the strong lateral exchange over the shoal represents an important pathway for the exchange of material between the sub-pycnocline waters in the channel and the surface. The fact that values of Ri are not observed to fall below 0.25 at mid–water column locations over the deeper channel for two complete tidal cycles suggests that there is little direct turbulent exchange across the pycnocline at this location (Miles 1961; Howard 1961). However, the combination of vigorous turbulent mixing throughout the water column during the ebb over the western shoal, combined with strong lateral circulation during the flood, provides an alternative pathway for the vertical exchange of materials. Lateral velocities in excess of 10 cm s^{-1} were consistently observed during flood tides by the moored ADCP. In a narrow estuary such as the Hudson River, these velocities could easily exchange materials between the deep channel and the adjacent shoal during the course of a single flood tide. This lateral advective pathway allows continued exchange between the deep water below the pycnocline and the overlying surface waters, even when persistent stratification prevents direct turbulent mixing through the pycnocline.

To help generalize the relative importance of lateral advection to vertical mixing in other systems, it is useful

to estimate the time scale for exchange driven by these two processes. The time scale of lateral advection can be represented as the estuarine width W divided by the magnitude of the lateral flow V. In a stratified estuary, the lateral momentum balance is largely geostrophic at tidal time scales, with the lateral flow driven by the higher-order ageostrophic terms (Scully et al. 2009). For this condition, Lerczak and Geyer (2004) present a scaling for the lateral flow,

$$V = \frac{1}{8}\frac{f}{\omega}U_t, \tag{7}$$

where f is the Coriolis parameter, ω is the tidal frequency, and U_t is the magnitude of the along-channel tidal current. The time scale for lateral exchange is then

$$T_{\text{adv}} = \frac{8\omega W}{fU_t}. \tag{8}$$

The time scale for vertical mixing can be presented as

$$T_{\text{mix}} = \frac{H^2}{K_z} = \frac{H^2N^2}{Rf\varepsilon}, \tag{9}$$

where K_z is the eddy diffusivity ($K_z = N^2/B$). Again, the buoyancy flux B is related to ε through the flux Richardson number. The ratio of these two time scales then becomes

$$\frac{T_{\text{mix}}}{T_{\text{adv}}} = \frac{H^2N^2fU_t}{8Rf\varepsilon\omega W}. \tag{10}$$

When this ratio is greater than one, the time scale of vertical mixing is longer than the time scale for lateral advection and advection is expected to contribute significantly to vertical exchange processes. For average values observed in the Hudson River ($H = 15$ m, $N^2 = 4 \times 10^{-3}$ s^{-2}, $U_t = 1$ m s^{-1}, and $\varepsilon = 1 \times 10^{-5}$ m^{-2} s^{-3}), this ratio is approximately 30, suggesting that lateral advection plays a key role in the vertical exchange during stratified conditions.

Many systems like the Hudson transition from strongly stratified to nearly well mixed over a spring–neap cycle. The reduced stratification and commensurate increase in dissipation associated with energetic tidal conditions will clearly favor vertical mixing over lateral exchange. Under well-mixed conditions, these systems also are more likely to demonstrate periodic stratification consistent with the traditional model of longitudinal tidal straining. Under well-mixed conditions, the longitudinal advection of stratification vanishes and lateral density gradients are reduced, which both contribute significantly to the observed patterns of stratification discussed above. The importance of lateral processes is highlighted in the Hudson because of its relatively narrow width. This not only reduces the advective time scale for lateral exchange but also enhances lateral gradients in $\partial S/\partial z$ that are important to the lateral advection of stratification.

The importance of lateral advective processes will be diminished in wide estuarine systems at tidal time scales. However many wide estuarine systems can be significantly impacted by wind forcing at synoptic times scales (~3 days). At these longer time scales, even relatively weak lateral flows can lead to significant channel–shoal exchange. Malone et al. (1986) suggest that wind-driven lateral circulation in Chesapeake Bay may play an important role in supplying nutrients from the subpycnocline waters to the surface layer, providing fuel for surface primary production. More recent work in Chesapeake Bay suggests that wind-driven lateral exchange between the channel and shoal may be the dominant mechanism for providing oxygen to hypoxic subpycnocline waters during the stratified summer months (Scully 2010). Many estuarine systems are persistently stratified, preventing significant turbulent flux through the pycnocline. For these systems, advective processes may provide the only transport pathway between surface and bottom waters.

Acknowledgments. We thank three anonymous reviewers for their thoughtful comments on this manuscript. The funding for this research was obtained from NSF Grant OCE-08-25226.

REFERENCES

Aris, R., 1956: On the dispersion of a solute in a fluid flowing through a tube. *Proc. Roy. Soc. London,* **235A,** 67–77.

Burchard, H., and R. D. Hetland, 2010: Quantifying the contribution of tidal straining and gravitational circulation to residual circulation is periodically stratified tidal estuaries. *J. Phys. Oceanogr.,* **40,** 1243–1262.

Chant, R. J., W. R. Geyer, R. H. Houghton, E. Hunter, and J. Lerzcak, 2007: Estuarine boundary layer mixing processes: Insights from dye experiments. *J. Phys. Oceanogr.,* **37,** 1859–1877.

Chatwin, P. C., 1976: Some remarks on the maintenance of the salinity distribution in estuaries. *Estuarine Coastal Mar. Sci.,* **4,** 555–566.

Elder, J. W., 1959: The dispersion of marked fluid in turbulent shear flow. *J. Fluid Mech.,* **5,** 544–560.

Fisher, H. B., 1976: Mixing and dispersion in estuaries. *Annu. Rev. Fluid Mech.,* **8,** 107–133.

Geyer, W. R., 1993: The importance of suppression of turbulence by stratification on the estuarine turbidity maximum. *Estuaries,* **16,** 113–125.

——, J. H. Trowbridge, and M. M. Bowen, 2000: The dynamics of a partially mixed estuary. *J. Phys. Oceanogr.,* **30,** 2035–2048.

——, M. E. Scully, and D. K. Ralston, 2008: Quantifying vertical mixing in estuaries. *Environ. Fluid Mech.,* **8,** 495–509.

Giddings, S. N., D. A. Fong, and S. G. Monismith, 2011: Role of straining and advection in the intratidal evolution of stratification, vertical mixing, and longitudinal dispersion of a shallow, macrotidal, salt wedge estuary. *J. Geophys. Res.,* **116,** C03003, doi:10.1029/2010JC006482.

Grant, W. D., A. J. Williams, and S. M. Glenn, 1984: Bottom stress estimates and their prediction on the Northern California continental shelf during CODE-1: The importance of wave-current interaction. *J. Phys. Oceanogr.,* **14,** 506–527.

Hansen, D. V., and M. Rattray, 1965: Gravitational circulation in straights and estuaries. *J. Mar. Res.,* **23,** 104–122.

Howard, L. N., 1961: Note on a paper by J.W. Miles. *J. Fluid Mech.,* **10,** 509–512.

Jay, D. A., and D. J. Smith, 1990: Circulation, density distribution and neap-spring transitions in the Columbia River estuary. *Prog. Oceanogr.,* **25,** 81–112.

——, and J. D. Musiak, 1994: Internal tidal asymmetry in channel flows: Origins and consequences. *Mixing in Estuaries and Coastal Seas,* C. Pattiaratchi, Ed., Coastal and Estuarine Studies, Vol. 50, Amer. Geophys. Union, 211–249.

Lacy, J. R., M. T. Stacey, J. R. Burau, and S. G. Monismith, 2003: Interaction of lateral baroclinic forcing and turbulence in an estuary. *J. Geophys. Res.,* **108,** 3089, doi:10.1029/2002JC001392.

Lerczak, J. A., and W. R. Geyer, 2004: Modeling the lateral circulation in straight, stratified estuaries. *J. Phys. Oceanogr.,* **34,** 1410–1428.

Lucas, L. V., J. E. Cloern, J. R. Koseff, S. G. Monismith, and J. K. Thompson, 1998: Does the Sverdrup critical depth model explain bloom dynamics in estuaries? *J. Mar. Res.,* **56,** 375–415.

Malone, T. C., W. M. Kemp, H. W. Ducklow, W. R. Boynton, J. H. Tuttle, and R. B. Jonas, 1986: Lateral variation in the production and fate of phytoplankton in a partially stratified estuary. *Mar. Ecol.,* **32,** 149–160.

Miles, J. W., 1961: On the stability of heterogeneous shear flows. *J. Fluid Mech.,* **10,** 496–508.

Moum, J. N., 1996: Efficiency of mixing in the main thermocline. *J. Geophys. Res.,* **101,** 12 057–12 069.

Nepf, H. M., and W. R. Geyer, 1996: Intra-tidal variations in stratification and mixing in the Hudson estuary. *J. Geophys. Res.,* **101,** 12 079–12 086.

Nunes, R. A., and J. H. Simpson, 1985: Axial convergence in a well-mixed estuary. *Estuarine Coastal Shelf Sci.,* **20,** 637–649.

Oakley, N. S., 1982: Determination of the rate of dissipation of turbulent energy from simultaneous temperature and velocity shear microstructure measurements. *J. Phys. Oceanogr.,* **12,** 256–271.

Officer, C. B., R. B. Biggs, J. L. Taft, L. E. Cronin, M. A. Tyler, and W. R. Boynton, 1984: Chesapeake Bay anoxia: Origin, development, and significance. *Science,* **223,** 22–27.

Osborn, T. R. J., 1980: Estimates of the local rate of vertical diffusion from dissipation measurements. *J. Phys. Oceanogr.,* **10,** 83–89.

Peters, H., 1997: Observations of stratified turbulent mixing in an estuary: Neap-to-spring variations during high river flow. *Estuarine Coastal Shelf Sci.,* **45,** 69–88.

——, and R. Bokhorst, 2000: Microstructure observations of turbulent mixing in a partially mixed estuary. Part I: Dissipation rate. *J. Phys. Oceanogr.,* **30,** 1232–1244.

Proudman, J., 1953: *Dynamical Oceanography*. Wiley, 409 pp.

Rippeth, T. P., E. Williams, and H. J. Simpson, 2002: Reynolds stress and turbulent energy production in a tidal channel. *J. Phys. Oceanogr.,* **32,** 1242–1251.

Scully, M. E., 2010: Wind modulation of dissolved oxygen in Chesapeake Bay. *Estuaries Coasts,* **33,** 1164–1175.

——, and C. T. Friedrichs, 2007: The importance of tidal and lateral asymmetries in stratification to residual circulation in partially mixed estuaries. *J. Phys. Oceanogr.,* **37,** 1496–1511.

——, W. R. Geyer, and J. A. Lerczak, 2009: The influence of lateral advection on the residual circulation: A numerical modeling study of the Hudson River estuary. *J. Phys. Oceanogr.,* **39,** 107–124.

——, ——, and J. H. Trowbridge, 2011: The influence of stratification and nonlocal turbulent production on estuarine turbulence: An assessment of turbulence closure with field observations. *J. Phys. Oceanogr.,* **41,** 166–185.

Simpson, J. H., J. Brown, J. Matthews, and G. Allen, 1990: Tidal straining, density currents, and stirring in the control of estuarine stratification. *Estuaries,* **13,** 125–132.

——, E. Williams, L. H. Brasseur, and J. M. Brubaker, 2005: The impact of tidal straining on the cycle of turbulence in a partially stratified estuary. *Cont. Shelf Res.,* **25,** 51–64.

Stacey, M. T., and D. K. Ralston, 2005: The scaling and structure of the estuarine bottom boundary layer. *J. Phys. Oceanogr.,* **35,** 55–71.

——, S. G. Monismith, and J. R. Burau, 1999: Observations of turbulence in a partially stratified estuary. *J. Phys. Oceanogr.,* **29,** 1950–1970.

——, J. R. Burau, and S. G. Monismith, 2001: Creation of residual flows in a partially stratified estuary. *J. Geophys. Res.,* **106** (C8), 17 013–17 037.

Taylor, G. I., 1954: The dispersion of matter in turbulent flow through a pipe. *Proc. Roy. Soc. London,* **223A,** 446–468.

Trowbridge, J. H., W. R. Geyer, M. M. Bowen, and A. J. Williams, 1999: Near-bottom turbulence measurements in a partially mixed estuary: Turbulent energy balance, velocity structure, and along-channel momentum balance. *J. Phys. Oceanogr.,* **29,** 3056–3072.